Interfacial Properties of an Ionic Liquid by Molecular Dynamics

Berit Heggen,*[,†,‡] Wei Zhao,[†] Frédéric Leroy,[†] Anton J. Dammers,[§,⊥] and Florian Müller-Plathe[†]

Eduard-Zintl-Institut für Anorganische und Physikalische Chemie, Technische Universität Darmstadt, Petersenstrasse 20, 64287 Darmstadt, Germany, Max-Planck-Insitut für Kohlenforschung, Kaiser-Wilhelm-Platz 1, 45470 Mülheim an der Ruhr, Department of Chemical Engineering, Delft University of Technology, Julianalaan 136, 2628 BL Delft, The Netherlands, and Biometris — Applied Statistics, Wageningen University, P.O. Box 100, 6700 AC Wageningen, The Netherlands

Received: November 23, 2009; Revised Manuscript Received: February 20, 2010

We studied the influence of a liquid−vapor interface on dynamic properties like reorientation and diffusion as well as the surface tension of the ionic liquid 1-butyl-3-methylimidazolium hexafluorophosphate ([bmim][PF_6]) by molecular dynamics simulations. In the interfacial region, reorientation of a short molecular axis is slightly faster than that in the central layer, while that of the longer molecular axis is retarded. The molecular reorientation is well-described by a stretched exponential decay modeled by the Kohlrausch−Williams−Watts equation. Analysis of the average translational diffusion coefficient of molecules in a central layer shows consistency with the Vogel−Fulcher−Tamann equation in a temperature range from 300 to 380 K. A first-passage time analysis of the system at 380 K yields a more refined spatial characterization of translational diffusion perpendicular to the liquid−vapor interfaces. In the central region of the slab, the diffusion coefficient of cations is only marginally higher than that of anions, but close to an interface, this difference is much higher, up to 50%. Apparent activation energies for rotational and diffusional dynamics, respectively, were estimated assuming Arrhenius behavior. They indicate that reorientation of the long molecular axis depends on the diffusion ability, whereas for the reorientation of the short axis, no such correlation is observed. The results are in general agreement with the literature, with slightly overestimated absolute values. This applies as well for the surface tension, where, however, a dependence on the treatment of the electrostatics was found. Particle-mesh Ewald (PME) or reaction field (RF) and the treatment of bonds by constraints have an influence. If no bond constraints are applied, the results are consistent for both methods for the description of the electrostatics.

Introduction

Ionic liquids (IL) are kown as salts with low melting points (below 100 °C) and have gained extensive attention due to their promising applications in the chemical industry.[1] Often, they are composed of bulky organic cations like 1-alkyl-3-methylimidazolium or tetraalkylammonium and smaller inorganic anions like chloride, tetrafluoroborate, or hexafluorophosphate. Due to their properties such as negligible vapor pressure, thermal stability, and ionic conductivity, they are used in a number of processes, such as electrochemistry.[1] Their nonvolatility makes them particularly interesting as so-called "green solvents".[2,3] Because of the wide variety of ions which can be combined into numerous ILs, they are also regarded as designer solvents since their physical properties like viscosity or hydrophobicity can be tuned by choosing anions and cations accordingly.

1-butyl-3-methylimidazolium hexafluorophosphate ([bmim]-[PF_6], see Figure 1) is one of the most studied ILs, both experimentally and theoretically. It is thermally as well as air and water stable[4] and has a melting point of around 10 °C, which allows research over a broad liquid region.[5,6] Furthermore, it has already been shown that [bmim][PF_6] is suitable for electrochemical processes[7] or as a solvent for homogeneous catalysis.[8] In addition, it dissolves a wide range of compounds.[9] Most physical properties like viscosity, surface tension, diffusion coefficients, solubility, and the liquid- and gas-phase structure have been measured experimentally.[1,10] As an important tool, molecular dynamics (MD) can provide important information that experiment is not able to probe, examples being mechanisms of different processes at the molecular level, understanding of which would be crucial to designing functional ionic liquids. To date, MD simulations have been employed to investigate and understand various characteristics of ionic liquids.[11–19] Moreover, attention has been paid to the study of structural

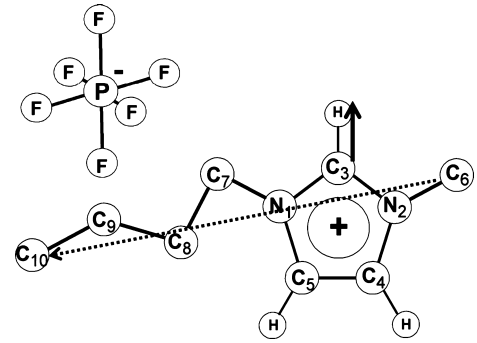

Figure 1. Representation of the ionic liquid [bmim][PF_6]. The arrows indicate the vectors C_3−H (solid) and C_6−C_{10} (dashed).

* To whom correspondence should be addressed. E-mail: heggen@mpi-muelheim.mpg.de.
[†] Technische Universität Darmstadt.
[‡] Max-Planck-Insitut für Kohlenforschung.
[§] Delft University of Technology.
[⊥] Wageningen University.

10.1021/jp911128j
Published on Web 05/04/2010

properties of ionic liquids through both experimental[20] and theoretical approaches.[12,14–17,19] However, very little has been done to examine the dynamic properties of the liquid−vapor interface of ionic liquids.

The aim of this work is to study at the molecular level the properties of an ionic liquid system containing a liquid−vapor interface (or, rather, a liquid−vacuum interface, given the low vapor pressure of Ils) by molecular dynamics simulations. Extensive efforts were made to understand the influence of the interface on the structural and dynamic properties as well as to calculate the surface tension. Temperature dependencies of these properties were also investigated.

Model and Methods

Model. Lopes and Pádua first published an all-atom force field for the treatment of Ils.[13] Their parameters were slightly modified by Bhargava and Balasubramanian by introducing a partial charge model in order to optimize the structure with respect to results from Car−Parrinello MD simulations as well as to reproduce experimental results like density, self-diffusion coefficients, and surface tension.[11] Note that in this force field, the net ion charges are reduced from ±1 to ±0.8 e. This reduction of the influence of the Coulombic interactions on the potential considerably improves the dynamic properties of the model, as shown before.[21] These modified force field parameters were used in this study. The van der Waals interactions were described by a Lennard-Jones potential with a cutoff distance of $r_{cutoff} = 1.2$ nm. The mixed Lennard-Jones parameters were calculated from the self-parameters ε_i and σ_i using the Lorentz−Berthelot mixing rules.[22] The Coulombic interactions have been treated either by the reaction field (RF) method[23] with an interaction cutoff distance of $r_{cutoff} = 1.2$ nm or by the particle-mesh Ewald (PME)[24] method with a cutoff distance of $r_{cutoff} = 1.2$ nm.

For comparison, we have run simulations with harmonic bond terms (parameters as in ref 11) and with holonomic bond constraints (the constraint distance is the same as the equilibrium distance of the harmonic bond term). Unless mentioned otherwise, the results reported are for the system with constraints.

Simulation Details. The system studied was made up of a rectangular box with a quadratic base in the x and y directions (4.46 nm) and an elongated z-axis (four times the base, 17.84 nm). This box was filled with 512 ion pairs of [bmim][PF_6], forming the liquid phase. Half of the box was empty to enable the study of the liquid−vacuum interface. Consequently, the liquid phase was effectively located in a slab of finite thickness, bound by two liquid−vapor interfaces. Initially, this box was built by merging two equilibrated bulk systems of 256 ion pairs. The vacuum part was added by elongating the z-axis of the resulting box. The system was studied at 300, 320, 340, 360, and 380 K applying *NVT* conditions. Periodic boundary conditions were applied. Additionally, the equilibrated bulk system (cubic periodic boundary conditions; no vacuum) of 256 ion pairs was used as input for a production run of 4 ns, which was used as the bulk reference system at 300 K.

For most simulations, the simulation package YASP[25,26] was used. As Ewald methods are not implemented in YASP, the simulation package Gromacs[27] was applied for some extra investigations. To allow comparison, a simulation setup as similar as possible was chosen for both programs. The time step was set to 0.002 ps and the atomic interaction cutoff radius to 1.2 nm. The temperature was kept constant by the Berendsen thermostat.[28] The coupling time was set to 0.2 ps. While in YASP the electrostatics can only be treated with a RF, Gromacs offers the choice between RF and PME. RF calculations were carried out using a reaction field dielectric constant of 11.4, which is the experimental value for [bmim][PF_6].[29]

The system was equilibrated with YASP for 1.5 ns at all temperatures. The YASP simulations were then run for 24.2 ns at 300 K, for 18.2 ns at 320 K, for 11.2 ns at 340 K, for 12.6 ns at 360 K, and for 14 ns at 380 K. Simulations with Gromacs were done for 8 ns. These simulations were only used for comparison in the discussion of the surface tension, which shows good convergence in this time.

For the analysis of the influence of the interface on various properties, the box was separated into layers perpendicular to the z-axis. Two interface layers were defined, each of 0.5 nm thickness, 0.5−1.0 nm (layer 1.0 nm) and 1.5−2.0 nm (layer 2.0 nm), always measured from the outermost atom. The central layer was defined as a layer of 4 nm placed around the center of the liquid phase. It was at least 2.5 nm away from either interface.

Results

Radial Distribution Function. The radial distribution functions (RDFs) were calculated between anions and anions, cations and anions, and cations and cations. As reference points, the centers of mass were chosen for the anions and the centers of mass of the five ring atoms for the cations. In our analysis, the RDFs were investigated for the entire liquid phase as well as separately for the interface layers and the central layer. No significant influence of the interface on the RDF could be found. This is also supported by the good agreement with the RDF for the reference bulk system and already published RDFs.[30] The temperature only marginally affects the radial distribution (results are not shown).

Ion Reorientation. For unit vectors (**u**) in the direction of the long axis C_6-C_{10} and the short axis C_3-H (Figure 1) as well as along P−F bonds, the reorientation correlation functions were calculated. The correlation function $c_1(t)$ is defined as

$$c_1(t) = \langle \mathbf{u}(t)\cdot\mathbf{u}(0)\rangle = \langle \cos\varphi(t)\rangle \quad (1)$$

where φ is the angle between the unit vector **u** at time 0 and at time t. The calculations were performed on four subtrajectories of lengths of 6 ns for the vector C_6-C_{10} and averaged over these four subtrajectories. For the vectors C_3-H and P−F, a shorter interval was used due to the faster reorientation; therefore, averaging over 15 subtrajectories of a length of 1.4 ns in the case of C_3-H and 0.7 ns for the anion vector was possible.

The relaxation time τ is the integral over the reorientation correlation function

$$\tau = \int_0^\infty c_1(t)\,\mathrm{d}t \quad (2)$$

In Figure 2−4, the logarithms of the correlation functions for the cations (C_6-C_{10}, C_3-H) and anions at 300 K are shown. The correlation functions were calculated as an average over the whole liquid phase, denoted as average, as well as separately for the individual layers described above. The ions were classified as belonging to one specific layer at the first time step. This is thought to be an approximation. We are aware of the fact that some ions might move out of the slab in the respective time step. However, regarding the diffusion coefficients, they stay in the proximity of the respective layers.

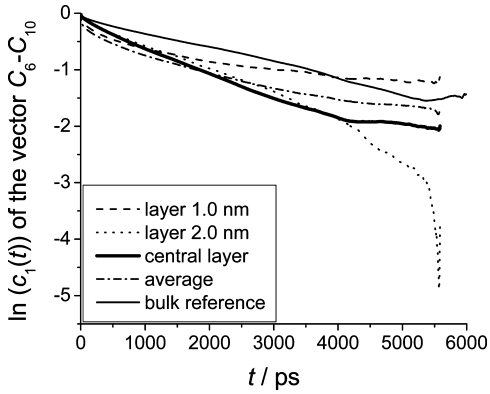

Figure 2. Semilogarithmic plot of the reorientation correlation function $c_1(t)$ for the cation vector C_6-C_{10} (long axis) at 300 K.

TABLE 1: Kohlrausch−Williams−Watts (see eq 3) Fitting Parameters and Rotational Relaxation Times τ (eq 2) at 300 K

vector	KWW parameters	layer 0.5−1.0 nm	layer 1.5−2.0 nm	central layer	bulk reference
C_6-C_{10}	β	0.41	0.85	0.74	0.83
	θ/ns	3.09	1.92	1.83	3.48
	τ/ns	9.55	2.08	2.20	3.83
C_3-H	β	0.49	0.44	0.46	0.42
	θ/ns	0.06	0.07	0.10	0.12
	τ/ns	0.11	0.17	0.24	0.34
P−F	β	0.83	0.83	0.82	0.78
	θ/ps	5.76	6.76	6.82	7.89
	τ/ps	6.36	7.52	7.60	9.13

In Figure 2, it is obvious that the reorientation process shows a steeper descent in the beginning and flattens over time, as would be expected for reorientation due to rotational diffusion.[31] In the layers close to the interface, this effect is stronger than that in the central layer. The slowest initial relaxation occurs in the bulk reference. The relaxation of molecular liquids often shows an exponential decay (Debye rotational diffusion). For the present ionic liquid, we find the reorientation to be well-described by a stretched exponential (Kohlrausch−Williams−Watts (KWW) function[32])

$$\ln c_1(t) \approx -\left(\frac{t}{\theta}\right)^{\beta} \tag{3}$$

where θ is the KWW time and the stretching factor β is less than 1, indicating that the exponential decay is retarded. The parameters found by a least-squares fit are given in Table 1. The long vector C_6-C_{10} (Figure 2) shows a different behavior compared to the short cation vector C_3-H (Figure 3). For the vector C_6-C_{10}, the parameter β increases from about 0.4 at the interface to around 0.7−0.8 in the central layer. For the perpendicular vector (C_3-H), it is almost constant throughout all layers at around 0.4. For the anions, β is in the range of 0.8 everywhere in the liquid phase (Figure 4; Table 1). The reorientation correlation for the near-spherical symmetric anions is almost similar to the behavior of neutral small-molecule liquids well above their melting points, which approach $\beta = 1$ (exponential decay). The relaxation times τ calculated by eq 2 are considerably smaller for the anions than those for the cations (Table 1). The difference is about 2 to 3 orders of magnitude; it is around 7 ps for the anions but in the range of 2−10 ns for the long axis of the cations (C_6-C_{10}) and somewhat smaller in the perpendicular direction at around 0.1−0.2 ns. The anions

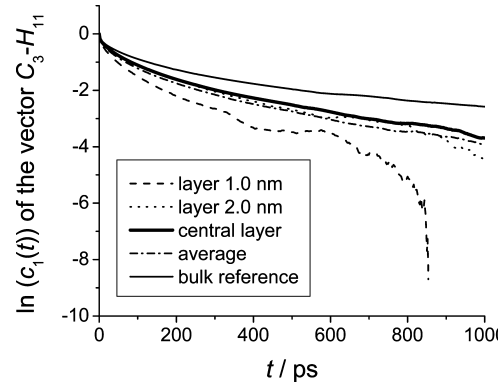

Figure 3. Semilogarithmic plot of the reorientation correlation function $c_1(t)$ of the vector C_3-H (short axis) at 300 K.

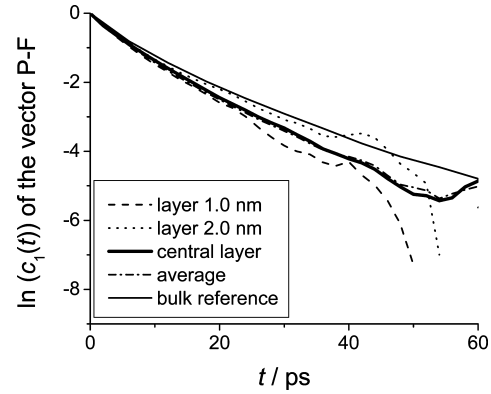

Figure 4. Semilogarithmic plot of the reorientation correlation function $c_1(t)$ of the anion vector P−F at 300 K.

show slightly slower reorientation in the central layer than that close to the interface (difference of about 1 ps). This tendency is apparent for the short cation vector C_3-H too. On the contrary, the long cation vector C_6-C_{10} reorients the slowest in the interface region, with about 10 ns decreasing to 2 ns in the central layer.

Comparison of the results for the central layer with those from the bulk reference system shows good agreement for the anions (almost the same β value; relaxation time 2 ps higher in the bulk reference system) and the short cation vector C_3-H (only the relaxation time is raised by about 0.1 ns in the bulk reference system). For the long cation vector, the difference is bigger (about 1.5 ns for the relaxation time; comparable β value). A possible explanation for the differences in reorientation between the layers is the ordering effect induced by the interface as pointed out by Lynden-Bell and del Popolo[19] and Bhargava and Balasubramanian.[16] They showed that the cations close to the interface orient themselves with the vector C_6-C_{10} along the interface normal with the butyl chain pointing toward the vapor phase. This ordering, which is known from surfactant molecules on water surfaces, may slow down the rotational dynamics. The short vector C_3-H appears to be considerably more mobile than the long molecular vector, most likely due to the smaller free volume required to permit a rotation of the cation around this molecular axis.

The temperature dependence of the reorientation parameters is small for the anions but more pronounced for the cations. In general, β remains almost constant with temperature. However, the reorientation time τ decreases with increasing temperature, as can be seen in Figure 5 for the vector C_6-C_{10}. The speeding up of the relaxation is obvious. Via an Arrhenius plot (not shown), the activation energy for the reorientation can be

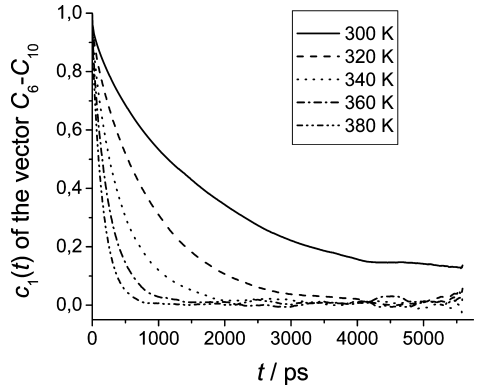

Figure 5. Temperature dependence of the reorientation correlation function $c_1(t)$ of the cation vector C_6-C_{10} (long axis) in the central layer.

calculated. Values of 31.2 (vector C_6-C_{10}) and 26.8 kJ/mol (vector C_3-H) are found for the cations, and 9.6 kJ/mol is found for the anions. The calculated activation energies for the cations are close to the activation energy of diffusion (about 35.8 kJ/mol; see below), indicating that the reorientation of the cations necessitates the displacement of neighboring ions, especially for the long vector C_6-C_{10}. In contrast, the energy barrier for the reorientation of the anions is three times smaller than that for self-diffusion, demonstrating that the anions can easily reorient in place. Similar differences have been found for the reorientation anisotropy of benzene molecules dissolved in polystyrene; the spinning around the C_6 axis proceeds in place with a low energy barrier, whereas the tumbling motion of a benzene molecule needs the creation of free volume and has a considerably higher activation energy.[33]

Antony et al. measured the reorientation dynamics of the vector C_3-H by NMR experiments.[10] They found a correlation time which was overall larger by a factor of 3 but showed comparable temperature dependence with an activation energy of 36.0 kJ/mol.

Self-Diffusion. For normal diffusion, the long-time behavior of the mean-square displacement (MSD) in a principal direction is given by the Einstein relation

$$\langle |r_i(t) - r_i(0)|^2 \rangle \approx 2D_{ii}t \tag{4}$$

where $r_i(t)$ is the i component ($i = x$, y or z) of the particle position $\mathbf{r}(t)$. Angular brackets denote an ensemble average. The diffusion coefficient D_{ii} can be obtained from the asymptotic slope of the MSD(t) curve as

$$D_{ii} = \frac{1}{2}\lim_{t\to\infty}\frac{\mathrm{d}}{\mathrm{d}t}\langle |r_i(t) - r_i(0)|^2 \rangle \tag{5}$$

The normal to the interfacial planes defines the z-axis. Accordingly, we use the notation $D_\perp = D_{zz}$. For diffusion in a direction parallel to the interface planes, the slab is effectively infinite and isotropic due to periodic boundary conditions. Hence, diffusion in the planar principal directions can be characterized by a single diffusion coefficient $D_\parallel = D_{xx} = D_{yy}$.

A directionally averaged diffusion coefficient is defined as

$$D_{\mathrm{av}} = \frac{1}{3}(\bar{D}_{xx} + \bar{D}_{yy} + \bar{D}_{zz}) = \frac{1}{3}(2\bar{D}_\parallel + \bar{D}_\perp) \tag{6}$$

where an overbar indicates averaging over initial particle positions throughout the full slab. Figure 6 shows D_{av} for cations as well as anions at a series of temperatures. Clearly, the data are reasonably well represented by an Arrhenius form

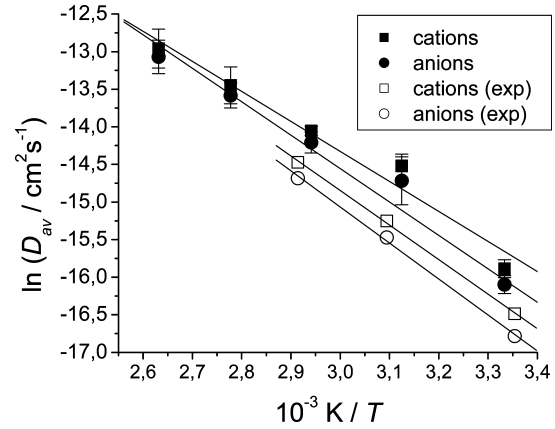

Figure 6. Dependence of the logarithm of the average self-diffusion coefficients D_{av} (filled symbols) and experimental values[34] (open symbols) on the inverse temperature. The linear fits are consistent with Arrhenius's law (eq 7).

TABLE 2: Vogel−Fulcher−Tamann Parameters (see eq 8) for Diffusion in [bmim][PF$_6$][a]

	$D_0/10^{-4}$ cm^2 s^{-1}	B/K	T_0/K
cations (central layer)	14	1804	103
cations (bulk reference)	0.6	621	206
cations (bulk, exper.)	1.8	1084	165
anions (central layer)	9.7	1621	111
anions (bulk reference)	0.5	664	203
anions (bulk, exper.)	1.5	987	169

[a] Values from this work and from experiments.[35]

$$D_{\mathrm{av}} = A\exp\left[-\frac{E_{\mathrm{A}}}{RT}\right] \tag{7}$$

with E_{A} as an activation energy and R as the molar gas constant. A linear fit of ln D_{av} versus $1/T$ yields activation energies of $E_{\mathrm{A}} = 35.8 \pm 2.4$ kJ/mol for cations and $E_{\mathrm{A}} = 36.9 \pm 2.4$ kJ/mol for anions. At all temperatures, the diffusion coefficient for cations is higher than that for anions. This is the same trend as observed in the bulk phase, both in simulations by Bhargava and Balasubramanian[11] and in experiments by Kanakubo et al.[34] using NMR spectroscopy. From the temperature dependence of the latter experimental diffusion coefficients, we deduced activation energies of $E_{\mathrm{A}} = 38.2$ kJ/mol for the cations and $E_{\mathrm{A}} = 39.8$ kJ/mol for the anions.

Tokuda et al.[35] analyzed the temperature dependence of the diffusion coefficients of several (bulk) ionic liquids in terms of the Vogel−Fulcher−Tamann (VFT) law

$$D = D_0\exp\left[-\frac{B}{T - T_0}\right] \tag{8}$$

essentially a generalization of the Arrhenius form eq 7. We calculated VFT fits of our simulation data, both for the bulk and in the slab for a central layer of thickness 4 nm. In the latter case, molecules were assigned to the layer by virtue of their initial positions. The associated fitting parameters T_0, B, and D_0 are given in Table 2, in conjunction with the experiment-related bulk values.[34] Data points and VFT fits are displayed in Figure 7. Our bulk simulations reproduce the experimental

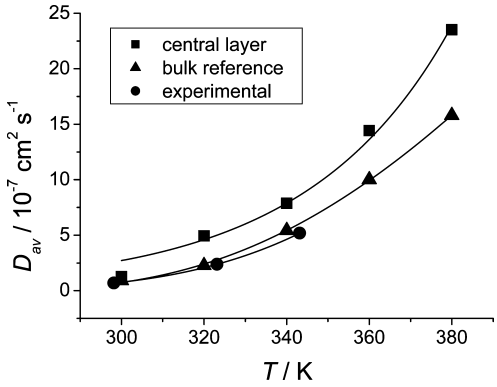

Figure 7. Vogel−Fulcher−Tamann fit for the diffusion coefficients of cations. Data are given for the central layer of this simulation, the bulk reference simulation, and experimental data.[35]

diffusion characteristics reasonably well. On the other hand, the diffusion coefficients related to molecules with an initial position in the central layer of the slab are consistently higher than the bulk values at the same temperature. A larger amount of available free volume or transient free volume might explain the faster dynamics in the slab relative to that in the bulk phase. As the liquid−vapor interfaces obviously play an important role in this behavior, a more refined spatially resolved analysis is of interest. Local diffusion coefficients are obtained by monitoring the trajectories of molecules initially present within a particular layer. At later times, however, these trajectories may extend into the surrounding liquid. Hence, the extracted diffusion coefficients do not strictly represent the dynamics of molecules in a layer, but rather, they reflect a mixture of properties of the layer and its environment.

A first attempt to study the ion mobility in a truly local, layer-resolved way was made by means of the lifetimes of contact pairs.[36] The results, however, turned out to be too erratic to be useful, probably due to insufficient statistics. Therefore, we will not elaborate on this analysis any further.

A promising alternative is a first-passage time (FPT) approach.[37] It was applied successfully to simulation studies of diffusion through nanometer-sized pores.[38] This included characterization of water permeation through a protein channel and observation of a gradient of the diffusion coefficient of water in a carbon nanotube, moving from the central region toward a channel end. The key question of the FPT phenomena is, how long does it take a particle, given its initial position, to reach a specific boundary for the first time? This can be interpreted as a virtual absorption process, where a particle, labeled at time $t = 0$, looses its identity upon reaching a boundary for the first time without, however, being removed physically. In our application, the faces of a liquid layer are natural candidates for such boundaries. Due to symmetry, diffusion parallel and perpendicular to these faces can be decoupled. Hence, the FPT problem can be mapped onto a one-dimensional diffusion problem in the z direction, with absorbing boundaries at $z = 0$ and $z = L$, respectively, where L is the layer thickness. It is governed by a diffusion coefficient $D_\perp$. Quantities of interest can be related to solutions of the diffusion equation with absorbing boundary conditions.[37]

We focus on the mean exit time $t(z_0)$, that is, the average time that it takes a particle, given its initial position $z(0) = z_0$, to leave the interval, either at $z = 0$ or at $z = L$. It is given by[37]

$$t(z_0) = \frac{1}{2D_\perp} z_0(L - z_0) \tag{9}$$

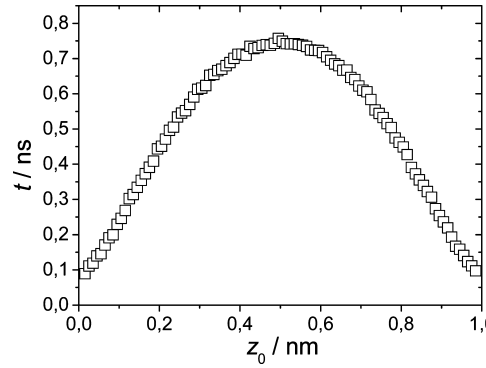

Figure 8. Mean exit time t of cations in a layer embedded in bulk [bmim][PF_6] at 380 K as a function of the initial particle position z_0. The layer thickness is $L = 1.0$ nm. The data are obtained by averaging 10 consecutive slabs with a moving step size of 0.1 nm.

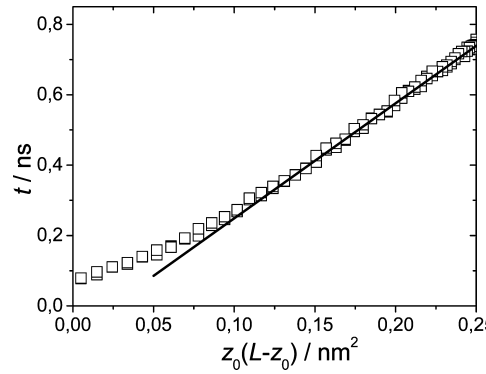

Figure 9. Mean exit time t of cations in a layer embedded in bulk [bmim][PF_6] at 380 K as a function of $z_0(L - z_0)$, where z_0 is the initial particle position. The layer thickness is $L = 1.0$ nm. Data points are the same as those in Figure 8. The solid line represents a linear fit in the region of 0.15 nm^2 < $z_0(L - z_0)$ < 0.25 nm^2. Its slope $1/2D_\perp$ (see eq 9) corresponds to $D_\perp = 1.51 \times 10^{-6}$ cm^2/s.

This is a parabola which crosses the z_0-axis at the boundary points $z_0 = 0$ and $z_0 = L$. It attains a maximum $L^2/8D_\perp$ at the center $z_0 = L/2$ of the interval. A parabolic fit to eq 9 of the simulation data gives us the diffusion coefficient $D_\perp$. Alternatively, $D_\perp$ can be obtained from the slope $1/2D_\perp$ of the linear representation $T(z_0)$ versus $z_0(L - z_0)$.

We applied the FPT analysis to the bulk liquid at 380 K. A layer thickness of $L = 1$ nm was chosen. The mean exit time $t(z_0)$ of cations as a function of the initial position z_0 is shown in Figure 8. The graph has a parabolic character, qualitatively consistent with eq 9. However, deviations are apparent near the boundaries. Indeed, the graph of $t(z_0)$ versus $z_0(L - z_0)$ (Figure 9) shows substantial nonlinearity in the region of $z_0(L - z_0)$ < 0.15 nm^2, corresponding to a "boundary layer" of roughly 0.2 nm wide. If we heuristically interpret the slope of the linear part in the region of 0.15 nm^2 < $z_0(L - z_0)$ < 0.25 nm^2 as $1/2D_\perp$, in accordance with eq 9, a diffusion coefficient of $D_\perp = (1.51 \pm 0.10) \times 10^{-6}$ cm^2/s is obtained. Alternatively, a MSD analysis (eq 5), applied to the full liquid box rather than just a layer, gives $D = (1.58 \pm 0.16) \times 10^{-6}$ cm^2/s for cations. This is essentially the same value as $D_\perp$, within the error bounds. A similar analysis for anions yields $D_\perp = (1.31 \pm 0.06) \times 10^{-6}$ cm^2/s, while the MSD-based value is $D = (1.24 \pm 0.03) \times 10^{-6}$ cm^2/s. Again, fair agreement between the two computational approaches is achieved.

At first sight, the mean exit time is consistent with a normal diffusion process if particles are launched at positions z_0 sufficiently far away from the boundaries. However, the linear

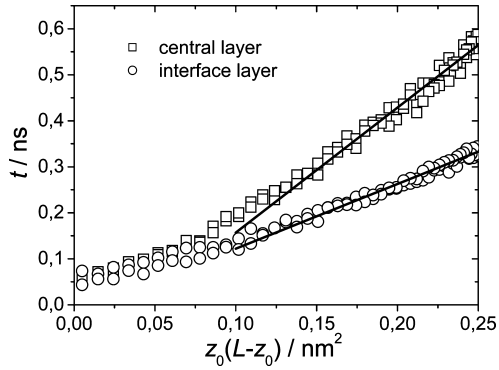

Figure 10. Mean exit time t of cations in two representative layers embedded in a slab of [bmim][PF_6] at 380 K as a function of $z_0(L - z_0)$, where z_0 is the initial particle position. The thickness of both layers is $L = 1.0$ nm. The solid lines represent linear fits in the region of 0.15 $nm^2 < z_0(L - z_0) < 0.25$ nm^2. From the slopes, the respective diffusion coefficients are obtained (see eq 9). Squares: central layer, $D_\perp = 1.84 \times 10^{-6}$ cm^2/s. Circles: interface layer, $D_\perp = 3.56 \times 10^{-6}$ cm^2/s.

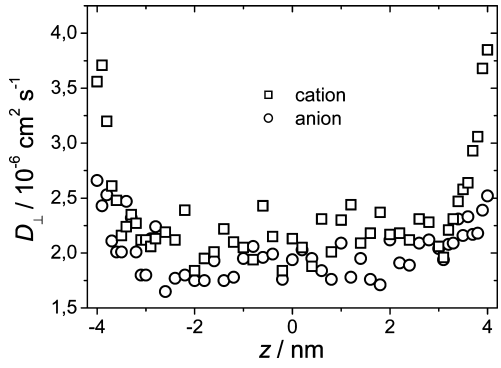

Figure 11. Spatial variation of the diffusion coefficients $D_\perp$ of cations and anions, respectively, in a slab of [bmim][PF_6] at 380 K. The total slab thickness is 8.9 nm.

part in Figure 9 does not extrapolate to $t = 0$ at the boundaries, but rather, it exhibits an offset. This may be qualitatively understood as follows. Schematically, the exit time of a particle is the sum of contributions from parts of its trajectory that traverse the boundary layer and parts that are located in a region further away from the boundary. Assuming that the average particle mobility in the boundary layer differs from regular diffusive behavior, this would explain a uniform offset for all particles launched far away from the boundary. An offset of the mean exit time of molecules was observed previously in various liquids, such as H_2O, Ar, and CO_2.[38,39] It was attributed to the finite velocity correlation time of molecules, well-known from the initial ballistic regime observed in the MSD. An absorbing boundary removes particles with an outgoing velocity, which results in significant deviations from an isotropic Maxwell−Boltzmann velocity distribution near the boundary. This causes a considerable offset of the mean exit time. However, in contrast to the observations in our IL system, apart from the offset, in these simple liquids, no significant distortions of the parabolic shape of $t(z_0)$ were observed. Ionic liquids, however, are known to also show aspects of supercooled dynamical behavior. Here, a subdiffusive interval, where $d(MSD(t))/dt < 1$, separates the ballistic and diffusive regimes.[40] This suggests that the observed deviation of $t(z_0)$ from parabolic behavior is related to supercooled or glassy dynamics. A further analysis, however, is beyond the scope of this paper.

The validation of the FPT methodology for bulk [bmim][PF_6] provides a basis for investigation of the liquid−vapor system, again at a temperature of 380 K. Within the liquid slab, we apply this procedure to layers of thickness $L = 1$ nm. The spatial profile of the mean exit time of cations for two representative layers is shown in Figure 10. The distance of the mid plane of the central layer to the center of the slab is 0.2 nm, while that of the surface layer is 4.0 nm. From the thickness of the liquid phase of 8.9 nm and the layer thickness of $L = 1.0$ nm, we readily deduce that the outer boundary of the surface layer has a distance of 0.4 nm from the liquid−vapor interface. Qualitatively, we observe the same diffusion characteristics as those in the bulk system (Figure 9). Clearly, the diffusion coefficients in the two layers are quite different, $D_\perp = (1.84 \pm 0.05) \times 10^{-6}$ cm^2/s for the central layer and $D_\perp = (3.56 \pm 0.08) \times 10^{-6}$ cm^2/s for the surface layer. A full profile of the diffusion coefficients as a function of the layer position within the liquid slab, for cations and ions, is given in Figure 11. We observe, within bounds set by statistical fluctuations, no significant spatial variation of $D_\perp$ in a central region of approximately 4 nm wide. Outside of this region, however, the diffusion coefficients of both types of ions increase upon approaching a liquid−vapor interface. Throughout the major part of the slab, the diffusion coefficient of cations is only marginally higher than that of anions. Close to the liquid−vapor interface, however, we observe a strong increase of $D_\perp$ for cations, whereas that of anions rises only moderately. This might result from two factors, (1) reduction of electrostatic cation−anion interactions due to the presence of the liquid−vapor interface or (2) alteration of the diffusion mechanism due to preorientation of cations at the interface. In the bulk and in the central layer, diffusional jumps of cations are coupled to the reorientation of the long axis C_6-C_{10}. Strong evidence is provided by very similar activation energies for both processes. Near the interface, however, their C_6-C_{10} vector is oriented in the z direction, and the butyl group points out of the liquid phase. This is known from the literature[16,19,41] and is also confirmed in the present simulations. Due to the preferentially parallel orientation, molecular displacements can proceed without reorientation either by exchange of neighboring ions (parallel diffusion) or by sliding in the direction of the molecular axis (perpendicular diffusion). In the latter case, the molecule has a low cross-sectional area or abutting face. Thus, there are mechanistic explanations for faster diffusion in both directions in the interface layer.

We also explored diffusion characteristics at temperatures below 380 K. Qualitatively, the same enhanced mobility near a liquid−vapor interface was observed, based on the characteristics of the mean exit time. However, upon decreasing the temperature, the boundary layer, allegedly attributed to anomalous diffusion, appeared to widen to such an extent that eventually, behavior consistent with normal diffusion was no longer visible. Indeed, as the temperature is lowered, the subdiffusive regime of the MSD as a function of time becomes more pronounced.[40] This phenomenon hampered a spatially resolved analysis at the full range of temperatures considered earlier.

Surface Tension. The surface tension γ was calculated from the diagonal elements p_{ii} of the pressure tensor[16]

$$\gamma = -\frac{L_z}{4}(p_{xx} + p_{yy} - 2p_{zz}) \tag{10}$$

where L_z is the length of the periodic box in the z direction.

In Figure 12, the dependence of the surface tension (YASP, RF method, bond constraints) on the temperature is shown and

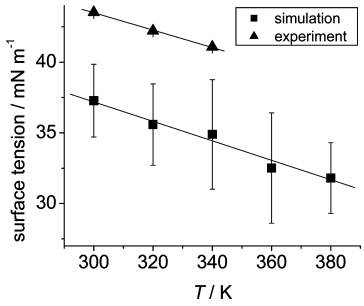

Figure 12. Dependence of the surface tension on temperature. Results from the YASP simulation with $\varepsilon_{RF} = 11.4$ (squares) and constraints and experimental values (triangles).[42] For the latter, the error bars are smaller than the symbols. The errors in the simulation are the standard deviation of the average values from the momentary values at each time step.

TABLE 3: Surface Tension Calculated at 300 K

method[a]	surface tension/mN m^{-1}
YASP, RF, with constraints	37.3 ± 2.6
YASP, RF, without constraints	44.7 ± 6.1
Gromacs, RF, with constraints	49.0 ± 1.2
Gromacs, RF, without constraints	49.3 ± 5.6
Gromacs, PME, with constraints	46.4 ± 1.5
experiment[42]	43.52

[a] RF: reaction-field approximation with $\varepsilon_{RF} = 11.4$. PME: particle-mesh Ewald.

compared to experimental results.[42] It is obvious that the surface tension obtained by simulation underestimates the experimental results at all temperatures. However, the general tendency of decreasing surface tension with increasing temperature is well-reproduced, as is the slope of this dependency.

In Table 3, the surface tensions at 300 K calculated with different methods are given. It is obvious that the surface tension depends on the precise details of the force fields (constraints versus flexible bonds) and the way of handling the electrostatic interactions (RF versus PME). The calculation with YASP using the RF method and the constrained bonds shows a clear underestimation of the experimental value, whereas with Gromacs, the respective value is too large. Obviously, the big differences between YASP and Gromacs are due to the constraints because the surface tension calculated with both programs becomes comparable if the bonds are treated as fully flexible. It is unlikely that this is caused by the different constraint algorithms (YASP uses SHAKE,[43] whereas Gromacs implements LINCS[44]). It is more probable that different ways of defining the virial (molecular versus atomic) cause a numerically different pressure anisotropy. The agreement with experiment is, in general, satisfactory for all schemes.

The surface tension of [bmim][PF_6] has also been calculated by Bhargava and Balasubramanian. They used the PME method and obtained a surface tension of 47 mN m^{-1}. Thus, they overestimated the experimental values with this method, as we did. From simulations of the molten salt potassium iodide, KI, Aguado et al. recommended using PME because it is necessary to avoid truncation effects in the long-range electrostatic interactions caused by a reaction field.[45] As the cutoff radius of 1.2 nm in our RF calculations is quite large, we neglect long-range corrections. It turns out, though, that those are quite necessary in the presence of interfaces due to truncations of the potential because of the inhomogeneity within the system. This is supported by the work of Pensado et al., showing that long-range corrections have an influence of about 10% on the value of the surface tension.[46] Moreover, in the literature, finite size effects causing variations of the surface tension are discussed.[47] It is suggested that one choose the size of the surface as (10 × diameter of the largest ion)^2. This is not the case in our simulations.

Conclusions and Outlook

In this work, we investigated the influence of a liquid−vapor interface on the properties of the ionic liquid [bmim][PF_6]. For the short-range structure measured by the radial distribution functions, no interface influence has been found. In contrast, dynamics like reorientation of the ions as well as their diffusion is influenced by the interface. The cations show faster reorientation close to the interface of the short molecular axis but slower reorientation of the long one compared to the central layer. In contrast, the diffusion is accelerated in the interfacial layer, possibly due to a preorientation of the cations, which point their butyl groups toward the vapor phase. This leads to a decoupling of translational and rotational motion of the ions. The reorientation process, in general, follows a Kohlrausch−Williams−Watts behavior.

In the central layer, the temperature dependence of both diffusion and reorientation is well-described by the Vogel−Fulcher−Tamann law. As the deviation from Arrhenius behavior is small, we can roughly estimate apparent activation energies in the interesting temperature range. The activation energies for diffusion and the reorientation of the long molecular axis of the cations are comparable, indicating that both processes are coupled and/or require a similar amount of available free volume. In contrast, the reorientation of the shorter cation axis and the anions has a lower activation energy, which is consistent with the picture of these reorientations occurring with much less redistribution of free volume, or even in place for the almost spherical anions. In general, the temperature dependencies are well-reproduced for all dynamical properties. In agreement with the literature, it was found throughout that the diffusion of the anions is slower than that of the cations.

The central layer was thought to represent bulk phase behavior. However, comparison to simulations of pure bulk phases shows some deviation for the dynamic properties. The dynamics in the central layer of the film is usually faster than that in the bulk liquid. As a reason, one may speculate that the inner part of the film is less compressed than a bulk ionic liquid. To achieve certainty, the liquid phase would have to be enlarged considerably to reduce effects of the interface on the behavior of the central layer, which is, however, beyond the scope of the present contribution.

The simulated surface tensions are comparable to previous experimental and theoretical work. However, the treatment of the electrostatics and constraints leads to variations. From our results, it is recommended not to apply bond constraints to prevent artifacts. Alternatively, one might think of other ways to estimate the surface tension. There is, for example, a thermodynamical method suggested by Gloor et al. for calculating the surface tension by free-energy perturbation, called the test-area technique.[48] This method is not as sensitive toward truncations of the potential. Besides, Yan et. al compared calculations of the surface tension of ionic liquids with nonpolarizable and polarizable force fields.[49] The polarizability is also thought to effect on dynamic properties.[50] They suggested that polarizable force fields are better at reproducing surface tension, which would help to improve the results as well. Additionally, a larger system might help to improve the results for the surface tension as well.

Acknowledgment. This work has been supported by the Priority Programmes 1191 "Ionic Liquids" and 1155 "Molecular Modelling and Simulation in Process Engineering" of the Deutsche Forschungsgemeinschaft. We thank the HHLR at TU Darmstadt for computer time.

References and Notes

(1) Weingärtner, H. *Angew. Chem., Int. Ed.* **2008**, *47*, 654.
(2) Brennecke, J. F.; Maginn, E. J. *AIChE J.* **2001**, *47*, 2384.
(3) Sheldon, R. A. *Green Chem.* **2005**, *7*, 267.
(4) Gannon, T. J.; Law, G.; Watson, P. R. *Langmuir* **1999**, *15*, 8429.
(5) Tokuda, H.; Tsuzuki, S.; Susan, M. A. B. H.; Hayamizu, K.; Watanabe, M. *J. Phys. Chem. B* **2006**, *110*, 19593.
(6) Kanakubo, M.; Ikeda, T.; Aizawa, T.; Nanjo, H.; Kameda, Y.; Amo, Y.; Usuki, T. *Anal. Sci.* **2008**, *24*, 1373.
(7) Halka, V.; Tsekov, R.; Freyland, W. *Phys. Chem. Chem. Phys.* **2005**, *7*, 2038.
(8) Sheldon, R. *Chem. Commun.* **2001**, 2399.
(9) Law, G.; Watson, P. R. *Langmuir* **2001**, *17*, 6138.
(10) Antony, J. H.; Mertens, D.; Dölle, A.; Wasserscheid, P.; Carper, W. R. *ChemPhysChem* **2003**, *4*, 588.
(11) Bhargava, B. L.; Balasubramanian, S. *J. Chem. Phys.* **2007**, *127*, 114510.
(12) Hunt, P. A. *Mol. Sim.* **2006**, *32*, 1.
(13) Lopes, J. N. C.; Padua, A. A. H. *J. Phys. Chem. B* **2006**, *110*, 19586.
(14) Lynden-Bell, R. M.; Popolo, M. G. d.; Youngs, T. G. A.; Kohanoff, J.; Hanke, C. G.; Harper, J. B.; Pinilla, C. C. *Acc. Chem. Res.* **2007**, *40*, 1138.
(15) Sloutskin, E.; Lynden-Bell, R. M.; Balasubramanian, S.; Deutsch, M. *J. Chem. Phys.* **2006**, *125*, 174715.
(16) Bhargava, B. L.; Balasubramanian, S. *J. Am. Chem. Soc.* **2006**, *128*, 10073.
(17) Bhargava, B. L.; Balasubramanian, S. *J. Phys. Chem. B* **2007**, *111*, 4477.
(18) Lopes, J. N. C.; Deschamps, J.; Pádua, A. A. H. *J. Phys. Chem. B* **2004**, *108*, 2038.
(19) Lynden-Bell, R. M.; Popolo, M. G. d. *Phys. Chem. Chem. Phys.* **2006**, *8*, 949.
(20) Lovelock, K. R. J.; Kolbeck, C.; Cremer, T.; Paape, N.; Schulz, P. S.; Wasserscheid, P.; Maier, F.; Steinrück, H.-P. *J. Phys. Chem. B* **2009**, *113*, 2854.
(21) Zhao, W.; Leroy, F.; Balasubramanian, S.; Müller-Plathe, F. *J. Phys. Chem. B* **2008**, *112*, 8129.
(22) Leach, A. R. *Molecular Modeling*, 2nd ed.; Pearson Prentice Hall: Harlow, U.K., 2001.
(23) Tironi, I. G.; Sperb, R.; Smith, P. E.; Gunsteren, W. F. v. *J. Chem. Phys.* **1994**, *102*, 5451.
(24) Darden, T.; York, D.; Pedersen, L. *J. Chem. Phys.* **1993**, *98*, 10089.
(25) Müller-Plathe, F. *Comput. Phys. Commun.* **1993**, *78*, 77.
(26) Tarmyshov, K. B.; Müller-Plathe, F. *J. Chem. Inf. Model.* **2005**, *45*, 1943.
(27) Lindahl, E.; Hess, B.; Spoel, D. v. d. *J. Mol. Model* **2001**, *7*, 306.
(28) Berendsen, H. J. C.; Postma, J. P. M.; Gunsteren, W. F. v.; DiNola, A.; Haak, J. R. *J. Chem. Phys.* **1984**, *81*, 3684.
(29) Wakai, C.; Oleinikova, A.; Ott, M.; Weingärtner, H. *J. Phys. Chem. B* **2005**, *109*, 17028.
(30) Zhao, W.; Leroy, F.; Heggen, B.; Zahn, S.; Kirchner, B.; Balasubramanian, S.; Müller-Plathe, F. *J. Am. Chem. Soc.* **2009**, *131*, 15825.
(31) Gordon, R. G. *J. Chem. Phys.* **1966**, *44*, 1830.
(32) Daguenet, C.; Dyson, P. J.; Krossing, I.; Oleinikova, A.; Slattery, J.; Wakai, C.; Weingärtner, H. *J. Phys. Chem. B* **2006**, *110*, 12682.
(33) Witt, R.; Sturz, L.; Dölle, A.; Müller-Plathe, F. *J. Phys. Chem. A* **2000**, *104*, 5716.
(34) Kanakubo, M.; Harris, K. R.; Tsuchihashi, N.; Ibuki, K.; Ueno, M. *J. Phys. Chem. B* **2007**, *111*, 2062.
(35) Tokuda, H.; Hayamizu, K.; Ishii, K.; Susan, M. A. B. H.; Watanabe, M. *J. Phys. Chem. B* **2004**, *108*, 16593.
(36) Müller-Plathe, F. *Macromolecules* **1996**, *29*, 4782.
(37) Redner, S. *A Guide to First-Passage Processes*; Cambridge University Press: New York, 2001.
(38) Hijkoop, V. J. v.; Dammers, A. J.; Malek, K.; Coppens, M.-O. *J. Chem. Phys.* **2007**, *127*, 085101.
(39) Dammers, A. J.; Hijkoop, V. J. v. To be published.
(40) Hu, Z.; Margulis, C. J. *Proc. Natl. Acad. Sci. U.S.A.* **2006**, *103*, 831.
(41) Ohno, A.; Hashimoto, H.; Nakajima, K.; Suzuki, M.; Kimura, K. *J. Chem. Phys.* **2009**, *130*, 204705.
(42) Freire, M. G.; Cavalho, P. J.; Fernandes, A. M.; Marrucho, I. M.; Queimada, A. J.; Coutinho, J. A. P. *J. Colloid Interface Sci.* **2007**, *314*, 621.
(43) Müller-Plathe, F.; Brown, D. *Comput. Phys. Commun.* **1991**, *64*, 7.
(44) Hess, B.; Bekker, H.; Berendsen, H. J. C.; Fraaije, J. C. E. M. *J. Comput. Chem.* **1997**, *18*, 1463.
(45) Aguado, A.; Wilson, M.; Madden, P. A. *J. Chem. Phys.* **2001**, *115*, 8603.
(46) Pensado, A. S.; Malfreyt, P.; Pádua, A. A. H. *J. Phys. Chem. B* **2009**, *113*, 14708.
(47) González-Melchor, M.; Bresme, F.; Alejandre, K. *J. Chem. Phys.* **2005**, *122*, 104710.
(48) Gloor, G. J.; Jackson, G. *J. Chem. Phys.* **2005**, *123*, 134703.
(49) Yan, T.; Li, S.; Jiang, W.; Gao, X.; Xiang, B.; Voth, G. A. *J. Phys. Chem. B* **2006**, *110*, 1800.
(50) Lynden-Bell, R. M.; Youngs, T. G. A. *J. Phys.: Condens. Matter* **2009**, *21*, 424120.

JP911128J